To cite this article: LIU X W, WAN D C. Hull form optimization of wave-making resistance in different speeds for a luxury cruise ship [J/OL]. Chinese Journal of Ship Research, 2020, 15(5). http://www.ship-research.com/EN/Y2020/V15/I5/1.

DOI: 10.19693/j.issn.1673-3185.01845

Hull form optimization of wave-making resistance in different speeds for a luxury cruise ship

LIU Xinwang[1,2,3], *WAN Decheng*[*1,2,3]

1 School of Naval Architecture, Ocean and Civil Engineering, Shanghai Jiao Tong University, Shanghai 200240, China

2 State Key Laboratory of Ocean Engineering, Shanghai Jiao Tong University, Shanghai 200240, China

3 Computational Marine Hydrodynamics Lab (CMHL), Shanghai Jiao Tong University, Shanghai 200240, China

Abstract: [**Objectives**] For the hull line optimization design of luxury cruise ships, except for its aesthetic needs, it is of utmost importance for the design and optimization of the hull form to be able to acquire resistance performance throughout the whole sailing period at variable speeds. This is in line with today's requirements of energy saving, safety, and comfort features. [**Methods**] Based on the in-house optimization design software OPTShip-SJTU for hull forms, a luxury cruise ship is regarded as the initial hull to reduce its wave-making resistance at variable speeds. The hull form deformation is then implemented by the free-form deformation (FFD) method and the resistance evaluation is carried out by the Neumann-Michell (NM) potential-flow-based solver NMShip-SJTU to obtain the optimal hull forms using optimization algorithms. Finally, the optimal hulls set at two specified speeds are then chosen for further analysis using the viscous-flow-based solver naoe-FOAM-SJTU in order to verify that the optimal hulls do have better total resistance performances at the two specified speeds. [**Results**] Results show that using NMShip-SJTU solver to do the optimization is more efficient and the two optimal hull forms have a 0.65% and 0.98% total resistance reduction respectively. [**Conclusions**] The research indicates that the simulation-based hull form optimization process can be applied in the optimization of resistance and even comprehensive performances for the luxury cruise ships.

Keywords: luxury cruise ships; multi-speed hull form optimization; wave-making resistance; OPTShip-SJTU; NM potential flow theory; naoe-FOAM-SJTU

CLC number: U661.71

0 Introduction

In the last 20 years, China has witnessed a rapid development of the shipbuilding industry and continuously improved shipbuilding technology, and a large number of ships of all types except luxury cruise ships have been successfully designed and built. Luxury cruise ships have been given the reputation of "Mobile City by Sea" due to their personalized interior design, land-based hierarchical layout, and diverse entertainment facilities; they are recognized by the international shipbuilding industry as "3-high" ships that integrate high technology, high added value, and high reliability, thereby leading to

Received: 2019 – 12 – 05 **Accepted**: 2020 – 04 – 26

Supported by: National Natural Science Foundation of China (51809169, 51879159); National Key R&D Program of China (2019YFB1704200, 2019YFC0312400); Chang Jiang Scholars Program of China (T2014099); Program of Excellent Academic Leaders in Shanghai City (17XD1402300); High-tech Ship Research Program of the Ministry of Industry and Information Technology of China

Authors: LIU Xinwang, male, born 1995, Ph.D. candidate. Research interest: optimization of comprehensive hydrodynamic performance of the ship and marine structures. E-mail: huhgf670@163.com

WAN Decheng , male, born 1967, Ph.D., professor, doctoral supervisor. Research interests: computational ship hydrodynamics, meshless particle method, hull form optimization, fluid-structure interaction, vortex-induced vibration/motion. E-mail: dcwan@sjtu.edu.cn

***Corresponding author**: WAN Decheng

high difficulty and cost in their design and construction. The focus of the shipbuilding industry in many developed countries has been shifted to luxury cruise ships; some European countries have always held a leading position in the design and construction of luxury cruise ships by virtue of their advantages in technology, experience, and equipment supply.

On Nov. 6, 2018, China State Shipbuilding Corporation (CSSC) officially signed the construction contract of the Vista-class cruise ship with a gross tonnage (GT) of 135 000 with American Carnival Group and Italian Fincantieri Group, marking the entrance of the substantive construction stage for the first large-scale cruise ship with advanced world level of China, and providing the foundation for independent design and construction of luxury cruise ships in China.

Compared with that of conventional ships, the structure of luxury cruise ships usually exhibits the following characteristics:

1) Principal dimensions: larger breadth and smaller depth; smaller block coefficient, and being slim below the waterline.

2) Bow and stern structures: square stern and bent bulbous bow, with forward-tilted and flaring stem post.

3) Propulsion mode: mostly driven by electricity; absence of main engine and propulsion shafting; small engine room; low vibration noise.

4) Aesthetic design: natural and beautiful for the parts above the waterline, and straightly aligned upper and lower structures.

However, due to the particularity of the hull form of luxury cruise ships (for example, commercial construction models are inaccessible), there are few relevant documents regarding the hydrodynamic performance, in particular, the optimization of resistance performance, of luxury cruise ships [1−3]; most available documents are optimizations for the routes and layouts of luxury cruise ships [4−7]. Therefore, it is necessary to carry out further research on the design and optimization of luxury cruise ships based on hydrodynamic performance, when the aforementioned characteristics of luxury cruise ships and strong demand for their design and construction in China are taken into account.

Based on the self-developed optimization design software for hull forms, OPTShip-SJTU, a luxury cruise ship is taken as the initial hull form and a free-form deformation (FFD) method is used to locally deform the bow, waterline, and stern in this paper. The resistance evaluation is performed by means of the wave-making resistance solver NMShip-SJTU that is based on Neumann-Michell (NM) potential flow theory, and the hull forms with the optimal wave-making resistance coefficients at different speeds are obtained by combining with the optimization algorithm. The optimized hull forms are further verified using the high-precision viscous flow solver, naoe-FOAM-SJTU, which has been extensively validated.

1 Characteristics and optimization design requirements of luxury cruise ships

A luxury cruise ship is not only a means of transportation, but also a place for travel and leisure, which determines that it exhibits higher requirements than general types of ships in terms of safety, comfort, energy saving, and environmental protection.

1) Safety: Based on the development of large-sized luxury cruise ships and the consideration of a large number of people on board, safety issues are attracting increasing attention. According to statistics, most accidents of luxury cruise ships have been caused by damage and fire. Therefore, the design of luxury cruise ships must not only meet the demands of the *International Convention for the Safety of Life at Sea* (SOLAS) [8] but also meet the requirements of *Safe Return to Port* (SRtP) [9]. According to the requirements, a ship should be able to safely return to the port on its own power, when a fire or flooding accident occurs within a certain safety limit. In this process, passengers can safely stay in the "safe area" and meet their basic needs; when the accident exceeds the safety limit, the important system is able to run for 3 hours to ensure orderly evacuation. It can be seen that sufficient power is a necessity. From the perspective of hydrodynamic performance, a ship will undoubtedly save power in case of emergency when it receives less resistance while sailing at a certain design speed.

2) Comfort: The comfort of a luxury cruise ship is primarily achieved by controlling the vibration and noise of the ship. Since luxury cruise ships are mostly driven by electricity, without the main engine and propulsion shafting, the vibration and noise generated in the engine room are small. Moreover, hydrodynamic noise cannot be ignored; for ex-

ample, the free-surface waves that arise when ships are sailing at medium and high speeds will generate hydrodynamic noise during their formation and propagation, thereby affecting the ornament and comfort of the cruise ship.

3) Energy saving and environmental protection: In order to build a "green" ocean, modern cruise ships all exhibit "clean" and "green" ship-class notations. In recent years, the international maritime organization (IMO) has successively released rules such as energy efficiency design index (EEDI) for controlling CO_2 emissions; these rules will greatly affect the design of luxury cruise ships. EEDI has put forward higher requirements for ship safety, environmental protection, energy efficiency, and crew health protection. In terms of the various hydrodynamic performances of ships, resistance performance undoubtedly exhibits the greatest impact on EEDI.

Therefore, ship design and optimization for resistance performance are particularly important for the hull form design of luxury cruise ships.

With the development of CFD technology and ship CAD technology, the hull form optimization design, based on numerical simulation, can be used to completely get rid of the conventional design mode. The technology takes a single or multiple optimal hydrodynamic performances of a ship as the design goal, and achieves the optimization solution for the ship hydrodynamic configuration, within the given constraints and configuration design space, by means of the technologies of CFD numerical simulation and modern optimization; eventually, the hull form with the best hydrodynamic performance under given conditions can be obtained.

A crucial part in the process of optimizing the hull form of luxury cruise ships based on hydrodynamic performance is the evaluation of hydrodynamic performance. According to the different methods of treating fluid viscosity in fluid mechanics, the methods of evaluating hydrodynamic performance can be divided into two categories: the potential-flow method based on the inviscid fluid assumption, and the viscous-flow method considering fluid viscosity. Although the potential-flow method adopts the inviscid fluid assumption, which deviates somewhat from the reality, the method is still widely used for problems in the field of ship design under some specific conditions, e.g., the use of frictional resistance and wave-making resistance to replace the total resistance of the ship; its biggest advantage is that it consumes much less calculation time and fewer resources while maintaining higher accuracy. It can be seen that this method is extremely suitable for the preliminary design and optimization of luxury cruise ships. The full-flow-field CFD method with viscosity being considered can restore the flow field more realistically, and achieve all the information about the flow field more conveniently; moreover, the method exhibits higher accuracy and reliability, and can assist or replace expensive ship model tests to some extent; however, the viscous-flow method consumes huge computational time and many resources when compared with the potential-flow method.

Huge progress has been made in hull form optimization and application all over the world [10−15]: optimized hull forms are transited from simple mathematical hull forms, standard models to practical hull forms; there are various hull form deformation methods; most of the objective functions are wave-making resistance, total resistance, stern wake uniformity, etc.; methods of evaluating hydrodynamic performance mainly include empirical formula, potential-flow method, RANS-based viscous-flow method, etc.; optimization algorithms include gradient-based optimization algorithms and intelligent optimization algorithms based on biological evolution; approximation models mainly involve Kriging, neural network, etc. However, most domestic applications rely on commercial software to build an optimization platform or evaluate hydrodynamic performance. Therefore, it is imminent to independently develop an optimization platform and perform hull form optimization on the basis of ship hydrodynamic performance, according to the demands of hull form optimization of luxury cruise ships.

For optimizing the resistance of a luxury cruise ship, the potential flow theory can be used to efficiently evaluate the wave-making resistance, and the wave-making resistance of the optimized hull form can be significantly reduced, thereby decreasing the total resistance of the luxury cruise ship. Meanwhile, it will reduce the free-surface wave and hydrodynamic noise of the ship, and improve its ornament and comfort. In addition, a luxury cruise ship is not designed and built only according to the design speed like ordinary ships, due to the specificity in use; instead, the ornament requests of the tourists on the cruise ship should be considered. For example, it needs to sail at a lower speed while passengers enjoy the beautiful sea scenery and underwater creatures; otherwise, it requires to slightly increase the ship speed to save more time. Therefore, the performance optimization in the design and construction of luxury cruise ships should be carried out not only for a single speed but also for multiple speeds.

In this paper, the software OPTShip-SJTU is used to optimize the wave-making resistance coefficient of a luxury cruise ship at two speeds (Fr= 0.171 15 and 0.209 18). Next, the FFD method is employed to perform the hull form deformation, and the wave-making resistance solver, NMShip-SJTU, is used to evaluate the resistance performance. Eventually, the multi-objective genetic algorithm is used to achieve the optimized hull form, and a viscous-flow-based CFD evaluation is performed to verify the reliability of the optimization results, thereby providing a reference for the optimization design of luxury cruise ships of the same type.

2 Modules and principle of hull form optimization software

Based on C++ language and the open-source platform, OpenFOAM, a hull form optimization design tool, OPTShip-SJTU, was independently developed by the Computational Marine Hydrodynamics Lab (CMHL), Shanghai Jiao Tong University. This software does not rely on other commercial software. It has integrated the modules of hull form deformation, hydrodynamic performance evaluation, approximation model construction, and optimization solution, which can implement automatic optimization design of hull form. The software framework is shown in Fig. 1.

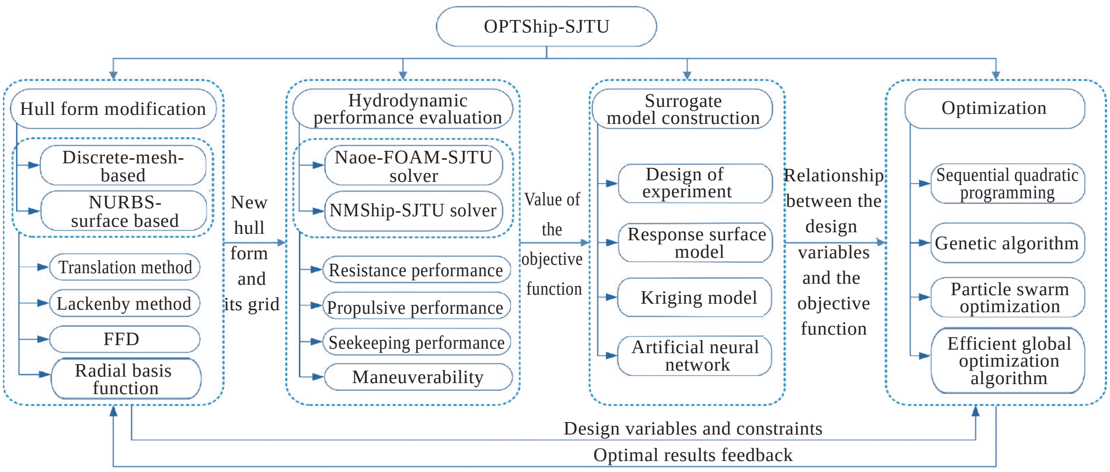

Fig. 1 Framework of OPTShip-SJTU hull form optimization software

2.1 Hull form deformation module

The FFD method was first proposed by Sederberg and Parry [16]. This method is analogous to that when the shell of an elastic object is deformed due to an external force, the geometrical entity embedded in it also undergoes a deformation. The FFD method is employed to transform the 3D entity according to similar steps: First, the area to be deformed is enclosed by a control body, which is equivalent to embedding the deformed object into the elastic control body; next, the shape of the control body is altered by moving the control vertices of the control body, which is equivalent to deforming the elastic body by an external force; eventually, the object to be deformed in the control body accordingly undergoes deformation as control points move. Fig. 2 shows the schematic diagram of the FFD method. The yellow point in Fig. 2 (a) constitute the initial control body, while the pink point and yellow point in Fig. 2 (b) represent the moving control points and fixed control points, respectively. The deformation of the bow can be implemented by means of this operation.

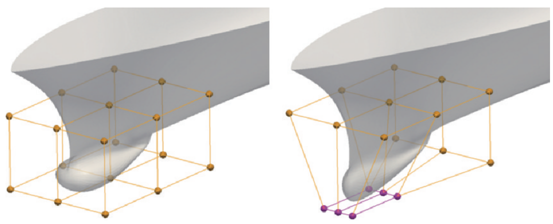

(a) Bow shape before deformation (b) Bow shape after deformation

Fig. 2 Schematic diagram of the FFD method

The control body of the FFD method can generally be chosen as a cuboid with (l+1), (m+1), and (n+ 1) control points being uniformly distributed in its length-, breadth-, and height-direction, respectively, and the cuboid is used to enclose the area to be deformed. The coordinates of the object to be deformed within the control body include global coordinates (*O-XYZ*) and local coordinates (*O'-STU*), as shown in Fig. 3.

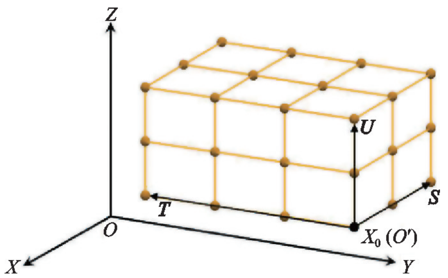

Fig. 3 Schematic diagram of global and local coordinate systems of the FFD method

A connection between the global coordinates of the object to be deformed within the control body and the global coordinates of the control point has been established by means of the following functional relationship:

$$\boldsymbol{X}(s,t,u)=\sum_{i=0}^{l}\sum_{j=0}^{m}\sum_{k=0}^{n}B_{i,l}(s)B_{j,m}(t)B_{k,n}(u)\boldsymbol{Q}_{i,j,k} \quad (1)$$

where $\boldsymbol{Q}_{i,j,k}$ stands for the global coordinates of a control point; $\boldsymbol{X}$ is the global coordinates of the object to be deformed within the control body; (s, t, u) represents the local coordinates of the object to be deformed within the control body; $B_{i,l}$, $B_{j,m}$, and $B_{k,n}$ stand for the lth-order, mth-order, and nth-order Bernstein polynomials, respectively. Take the first term, $B_{i,l}(s)$, as an example, the Bernstein polynomial is defined as

$$B_{i,l}(s)=\frac{l!}{i!(l-i)!}s^i(1-s)^{l-i} \quad (2)$$

It can be seen from Eq. (1) that global coordinates are employed to describe the geometric position of an object in space, and they can be expressed as a linear superposition of the products of the control point and the Bernstein polynomials; therefore, the global coordinates of the object to be deformed will also change while the control point are moved. The local coordinates represent the relative position between the object to be deformed within the control body and the point of the control body; once the control body is given, the coordinates (s, t, u) of the object to be deformed within the control body are determined, and will not change in the course of deformation.

When the control body is a regular cuboid, and the control vertices are uniformly distributed in the three directions, the local coordinates can be solved quickly by means of Eq. (3):

$$\boldsymbol{X}=\boldsymbol{X}_0+s\boldsymbol{S}+t\boldsymbol{T}+u\boldsymbol{U} \quad (3)$$

where $\boldsymbol{X}_0$ is the global coordinates of the origin of the control body; $\boldsymbol{S}$, $\boldsymbol{T}$, and $\boldsymbol{U}$ stand for the vectors in the direction of length, breadth, and height of the control body, respectively, as shown in Fig. 3. The local coordinates (s, t, u) of an arbitrary point can be solved by means of Eq. (4):

$$\begin{cases} s=\dfrac{\boldsymbol{T}\times\boldsymbol{U}\cdot(\boldsymbol{X}-\boldsymbol{X}_0)}{\boldsymbol{T}\times\boldsymbol{U}\cdot\boldsymbol{S}} \\ t=\dfrac{\boldsymbol{S}\times\boldsymbol{U}\cdot(\boldsymbol{X}-\boldsymbol{X}_0)}{\boldsymbol{S}\times\boldsymbol{U}\cdot\boldsymbol{T}} \\ u=\dfrac{\boldsymbol{S}\times\boldsymbol{T}\cdot(\boldsymbol{X}-\boldsymbol{X}_0)}{\boldsymbol{S}\times\boldsymbol{T}\cdot\boldsymbol{U}} \end{cases} \quad (4)$$

The global coordinates of the point of the control body can be achieved in accordance with Eq. (5):

$$\boldsymbol{Q}_{i,j,k}=\boldsymbol{O}'+\frac{i}{l}\boldsymbol{S}+\frac{j}{m}\boldsymbol{T}+\frac{k}{n}\boldsymbol{U} \quad (5)$$

where $i = 0, 1, ..., l$; $j = 0, 1, ..., m$; $k = 0, 1, ..., n$.

The calculation model in this work is obtained by generating the surface mesh of the hull according to the initial graphics exchange specification (IGES) file and then deforming the hull form by means of the FFD method. While moving the point of the control body through FFD method, one can achieve the global coordinates of an arbitrary point within the control body after deformation by substituting the local coordinates (s, t, u) obtained from the above calculation and the new coordinates of the control point into Eq. (1).

2.2 Hydrodynamic performance evaluation module

The NM method is used to solve ship wave-making problems. This method was proposed by Noblesse et al. [17] in 2013, and it is a method obtained by improving the Neumann-Kelvin (NK) theory. In the NK theory, the velocity potential at an arbitrary point in the flow field can be expressed as the sum of the integral of the wetted surface of the hull and the integral along the waterline of the hull. In particular, the integral along the waterline of the hull is a tough problem to solve, because it needs to consider the influence of the free surface and calculate the partial derivative of the velocity potential. The NM theory introduces a coordinated flow model and wave function and eliminates the term related to the integral along the ship waterline in NK theory through a series of mathematical transformations. In NM theory, the velocity potential at an arbitrary point in the flow field can be obtained by merely calculating the integral on the wetted surface of the hull. Fig. 4 shows the schematic diagram of the coordinate system of the NM theory.

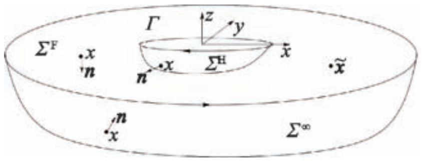

Fig. 4 Schematic diagram of the coordinate system of NM theory

The NM theory solves the velocity potential based on a Green's function method (GFM), which converts a boundary value problem into an integral problem for solving. According to Green's second identity, the boundary integral expression can be obtained.

$$\tilde{C}\tilde{\phi}=\int_{\Sigma}(G\boldsymbol{n}\cdot\nabla\phi-\phi\boldsymbol{n}\cdot\nabla G)\mathrm{d}a \tag{6}$$

where $\tilde{C}$ is the area contribution coefficient, whose specific value is determined according to the relative position between the field point and the boundary surface; $\tilde{\phi}$ is the velocity potential of field point; ϕ is the velocity potential of a point on the boundary surface; G is Green's function; $\boldsymbol{n}$ is the unit normal vector of the wetted surface of the hull, which is perpendicular to the hull surface and is pointing to the flow field; a is the micro-element area.

The boundary surface Σ is composed of the real wetted surface of the hull Σ^{H}, the real free surface Σ^{F}, and the infinite boundary Σ^{∞}. When field point $\tilde{\boldsymbol{x}}$ belongs to the interior of boundary surface Σ, $\tilde{C}$=1; when field point $\tilde{\boldsymbol{x}}$ belongs to the exterior of boundary surface Σ, $\tilde{C}$=0; when field point $\tilde{\boldsymbol{x}}$ is exactly located on the boundary surface Σ, $\tilde{C}$=0.5. Green's function G satisfies the following relationship:

$$4\pi G=-\frac{1}{r}+H(\tilde{\boldsymbol{x}};\boldsymbol{x}) \tag{7}$$

where $H(\tilde{\boldsymbol{x}};\boldsymbol{x})$ is the function representing the wave-making effect of the free surface, which is a harmonic function within the boundary surface Σ; r is the Euclidean distance between the field point $\tilde{\boldsymbol{x}}$ and the source point $\boldsymbol{x}$.

Green's function G will decay to 0 at infinity; therefore, the integrand in Eq. (6), i.e., the integral of $G\boldsymbol{n}\cdot\nabla\phi-\phi\boldsymbol{n}\cdot\nabla G$ over the infinite boundary surface Σ^{∞}, can be ignored. Moreover, according to the impermeable boundary condition of the wetted surface of the hull

$$\boldsymbol{n}\cdot\nabla\phi=n^{x} \tag{8}$$

Eq. (6) can be simplified as

$$\tilde{\phi}=\int_{\Sigma_a^{\mathrm{H}}}Gn^{x}\mathrm{d}a-\int_{\Sigma_a^{\mathrm{H}}}\phi\boldsymbol{n}\cdot\nabla G\mathrm{d}a+$$
$$\int_{\Sigma_a^{\mathrm{F}}}(G\boldsymbol{n}\cdot\nabla\phi-\phi\boldsymbol{n}\cdot\nabla G)\mathrm{d}a \tag{9}$$

When the influence of the free-surface nonlinear terms is ignored, and $\tilde{C}$=1 is temporarily taken, Eq. (9) can be further simplified as

$$\tilde{\phi}=\int_{\Sigma_a^{\mathrm{H}}}Gn^{x}\mathrm{d}a-\int_{\Sigma_a^{\mathrm{H}}}\phi\boldsymbol{n}\cdot\nabla G\mathrm{d}a+$$
$$F^{2}\int_{\Gamma}\frac{\phi G_{x}-G\phi_{x}}{\sqrt{(n^{x})^{2}+(n^{y})^{2}}}n^{x}\mathrm{d}l+\int_{\Sigma^{\mathrm{F}}}\left(\pi^{G}\phi-G\pi^{\phi}\right)\mathrm{d}x\mathrm{d}y \tag{10}$$

where G_x is the first-order partial derivative of G with respect to x; F is the Froude number (Fr); Γ is the line of intersection between the wetted surface of the hull and the mean free surface (namely the mean waterline); dl is the length micro-element on Γ; $\boldsymbol{n}\equiv(n^{x}, n^{y}, n^{z})$. π^{G} and π^{ϕ} are set to be the differential operators on G and ϕ, and they are respectively defined as

$$\pi^{G}\equiv G_{z}+F^{2}G_{xx},\ \ \pi^{\phi}\equiv\phi_{z}+F^{2}\phi_{xx} \tag{11}$$

where G_z is the first-order partial derivative of G with respect to z; G_{xx} is the second-order partial derivative of G with respect to x; ϕ_z is the first-order partial derivative of ϕ with respect to z; ϕ_{xx} is the second-order partial derivative of ϕ with respect to x.

Furthermore, according to the coordinated linear flow model, after mathematical derivation, Eq. (10) can be simplified as

$$\tilde{\phi}=\int_{\Sigma^{\mathrm{H}}}(Gn^{x}-\phi\boldsymbol{n}\cdot\nabla G)\mathrm{d}a+$$
$$F^{2}\int_{\Gamma}\frac{\phi G_{x}n^{x}\mathrm{d}l}{\sqrt{(n^{x})^{2}+(n^{y})^{2}}}+\int_{\Sigma^{\mathrm{F}}}\left(\pi^{G}\phi-G\pi^{\phi}\right)\mathrm{d}x\mathrm{d}y \tag{12}$$

Eq. (12) is the expression of the velocity potential of the flow field derived from the coordinated linear model in NM theory; it can be seen that $G\phi_x$ in the waterline integral is already eliminated in comparison with Eq. (10).

Green's function G is decomposed into the wave-making section W and the local flow section L; the wave-making section W satisfies the radiation condition, the Kelvin-Michell linear free-surface boundary condition, and the Laplace equation. A wave function $\boldsymbol{W}$ is introduced, and the wave-making section W and the wave function $\boldsymbol{W}$ satisfy $\nabla\times\boldsymbol{W}=\nabla W$; then, the wave function can be written as

$$\boldsymbol{W}=(0,W_{z}^{x},-W_{y}^{x}) \tag{13}$$

where subscripts z and y stand for the first-order partial derivatives of W in z- and y-direction, respectively; superscript x is the integral of x. By means of a series of mathematical transformations, the velocity potential expression with the term ϕG_x being eliminated can be achieved as

$$\tilde{\phi}=\tilde{\phi}_{\mathrm{H}}+\tilde{\psi}^{\mathrm{W}}+\tilde{\psi}^{\mathrm{L}} \tag{14}$$

It can be easily seen from Eq. (14) that the velocity potential in NM theory consists of two parts: the initial known term ($\tilde{\phi}_{\mathrm{H}}$) and the NM theory corrected term (including the wave-making correction $\tilde{\psi}^{\mathrm{W}}$ and the local flow correction $\tilde{\psi}^{\mathrm{L}}$).

It is known from theoretical analysis and the results of numerical calculation that the term of local flow correction $\tilde{\psi}^{\mathrm{L}}$ exhibits minor influence on the final calculation results, and the effect of this term is often ignored in practical applications. Therefore, the final simplified NM velocity potential can be expressed as

$$\tilde{\phi} \approx \tilde{\phi}_{\mathrm{H}} + \tilde{\psi}^{\mathrm{W}} \tag{15}$$

where

$$\tilde{\phi}_{\mathrm{H}} = \int_{\Sigma^{\mathrm{H}}} G n^x \mathrm{d}a - \int_{\Sigma^{\mathrm{F}}} G \pi^{\phi} \mathrm{d}x \mathrm{d}y \tag{16}$$

$$\tilde{\psi}^{\mathrm{W}} = \int_{\Sigma^{\mathrm{H}}} (-\phi_{t'} \boldsymbol{d}' + \phi_{d'} \boldsymbol{t}') \cdot \boldsymbol{W} \mathrm{d}a \tag{17}$$

where $\boldsymbol{t}'$ and $\boldsymbol{d}'$ are two unit vectors tangent to the wetted surface of the hull, which is respectively taken as

$$\begin{gathered} \boldsymbol{d}' = (0, -v^z, v^y), \quad \boldsymbol{t}' = (v, -n^x v^y, -n^x v^z) \\ v = \sqrt{(n^y)^2 + (n^z)^2}, \quad (v^y, v^z) = (n^y, n^z)/v \end{gathered} \tag{18}$$

On the port side of the hull, the unit vector $\boldsymbol{d}'$ points upward; on the starboard side of the hull, the unit vector $\boldsymbol{d}'$ points downward. At an arbitrary position of the hull, the unit vector $\boldsymbol{t}'$ always points to the bow, and $\boldsymbol{t}'$ and $\boldsymbol{d}'$ are always perpendicular to each other. $\phi_{t'}$ and $\phi_{d'}$ stand for the $\boldsymbol{t}'$- and $\boldsymbol{d}'$-component of the velocity on the wetted surface of the hull.

The use of the above formulas allows one to further forecast the ship wave-making resistance in still water, sinkage, trim, and free-surface wave elevation. This method can not only accurately predict the trend of ship resistance, but also consume short calculation time and small storage space, thereby making it very suitable for hull form optimization. Therefore, the wave-making resistance solver, NMShip-SJTU, which is independently developed on the basis of using the aforementioned method and C++ language, will be taken as the tool for the numerical calculation of wave-making resistance in this paper.

2.3 Module of approximation model construction for the response function

The quantity of numerical calculations related to the use of the aforementioned potential flow theory in ship hydrodynamics and hull form design is relatively large, and the introduction of methods of design of experiments (DoE) in hull form design can greatly improve the optimization efficiency while ensuring certain accuracy.

The DoE methods are used to determine the experimental design from the perspective of mathematical statistics, which can reduce the number of design samples while ensuring the accuracy of the sample population. With x_1 and x_2 being the design variables, Fig. 5 shows the uniform distribution sampling design, the random Latin hypercube sampling (LHS) design, and the optimized LHS design. It can be seen that the uniformity and orthogonality of the optimized LHS design are superior, and can better improve the calculation efficiency. Therefore, the optimized LHS design method is used to select the design samples of the new hull form in this work.

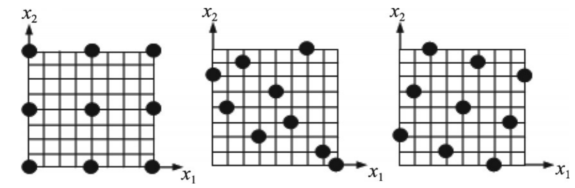

(a) Uniform distribution sampling design (b) Random LHS design (c) Optimized LHS design

Fig. 5 Schematic diagram of uniformity and orthogonality of different DoE methods

The Kriging approximation model [15] is the major model of the approximation function established in geostatistics; it was initially used in the mining field, and then gradually applied to multiple fields. The model is a method for unbiased and optimal estimation of variable values in accordance with the spatial correlation of the variables. Its basic idea is that the value of an unknown point is the mean value of its neighboring points, and the weight is the distance from the unknown point to the given points. From the perspective of interpolation, it is a method to achieve the linear optimal and unbiased interpolation estimation of spatially distributed data. The Kriging model has excellent adaptability and can be extensively used to approximate low-order and high-order nonlinear functions. Once the wave-making resistance of the new hull form chosen in the DoE is sequentially calculated, the response function that represents the relationship between the hydrodynamic parameters, such as the wave-making resistance coefficient, and the hull form parameters can be established according to the Kriging approximation model. In this paper, the response function will be used in hull form optimization.

2.4 Optimization solution module

When only one objective function exists, a global optimal solution can be found, which is superior to other solutions. When multiple targets coexist, there often exists conflicts between these targets, and it is hard to find a solution to optimize all the targets simultaneously. Therefore, there is a multi-objective optimization method with its essence of making at least one target better while without worsening any other targets; this multi-objective optimization method is termed as the optimization based on the Pareto front. For multi-objective optimization problems, there usually exists a solution set with the characteristic that there is no longer room for Pareto optimization for all the solutions within the set. This solution set is called the Pareto optimal solution set.

Non-dominated sorting genetic algorithm (NSGA) [18] adopts a non-dominated hierarchical method, and allows individuals with better performance to have a greater survival probability; its fitness sharing strategy is able to prevent "super individuals" from premature convergence due to over-reproduction. However, NSGA still has problems such as a lack of elite strategy and complex calculation. NSGA-II introduces an elite strategy to directly save the excellent parent individuals to the child population, and prevent the decrease of algorithm efficiency caused by the loss of excellent individuals. Moreover, the diversity of the population under the condition of elite strategy can be guaranteed by evaluating the population density around individuals with crowded comparison operators, and simultaneously choosing suitable individuals according to the non-dominated sorting and crowding. Therefore, NSGA-II has become one of the most popular and reliable multi-objective genetic algorithms, and it is also the multi-objective wave-making resistance optimization algorithm used in this paper.

3 A case study of the hull line optimization of a luxury cruise ship

3.1 Establishment of the optimization problem

In this paper, the optimization design for the wave-making resistance of the first home-made 135 000-ton Vista-class luxury cruise ship at two speeds (Fr=0.171 15 or 0.209 18) was carried out. The hull form and the principal dimensions of the ship are shown in Fig. 6 and Table 1, respectively.

Fig. 6 Front view of the luxury cruise ship

Table 1 Main dimensions of the luxury cruise ship

Parameter	Value
Scale ratio	1∶40
Froude number Fr	0.171 15, 0.209 18
Waterline length L_{wl}/m	7.458
Moulded breadth B/m	0.932
Moulded depth D/m	0.206

During optimization, the geometric reconstruction area needs to be carefully considered in order to affect the ship wave-making resistance. In consideration of the fact that the local deformation range has a minor influence on the wetted surface area of the entire ship, the total resistance is replaced by the wave-making resistance to optimize the target hull form. According to the principle described in the previous section, multi-objective optimization is applied to the objective functions, which are chosen as the wave-making resistance coefficients C_w at two speeds. That is to say, the objective functions are defined as

$$\min f_1 = C_w(Fr = 0.171\,15) \tag{19}$$

$$\min f_2 = C_w(Fr = 0.209\,18) \tag{20}$$

The FFD method is utilized to geometrically reconstruct the bow and stern, as shown in Fig. 7. The three lattices in the figure represent three FFD deformation areas, and the red line stands for the waterline. A detailed description is given below.

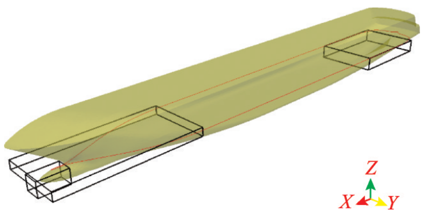

Fig. 7 Schematic diagram of FFD lattices of the luxury cruise ship

Firstly, since the bent bulbous bow of the luxury cruise ship can reduce its wave-making resistance, its shape can be optimized; a control body can be set in the bulbous bow area to implement the changes in the length, breadth and height of the bulbous bow. However, this luxury cruise ship exhibits a shallow draft, thereby leading to a small part of the bulbous bow above the water surface. It is necessary to keep the water entry points at the bulbous bow unchanged in order to ensure that the waterline length in the principal dimensions remains unchanged. This requires a limitation on the control points of the deformation lattice along the ship length and draft directions, so as to prevent the changes of water entry points in the ship length direction as well as the reduction of waterline surface caused by the immersion of the initial water entry points due to the deformation in draft direction.

Secondly, although the limitation on water entry points remains unchanged, a deformation lattice can be set in the vicinity of the waterline, but the moulded breadth must be kept unchanged, since the waterline width of the inflow section is variable, namely that the waterline of the entire bow (parallel to the front of midbody) can change in the ship breadth direction.

Eventually, a deformation lattice in the stern outflow section (parallel to the rear of midbody) is set, and according to the draft direction, the control points near the waterline and the control points of two cross-sections in the ship breadth direction are moved to comprehensively change the UV degree of the stern cross-section line.

The control point are uniformly distributed in each control body. In Fig. 8, the green and red control points stand for fixed and moving control points, respectively; the total number of design variables is 7, as shown in Table 2. In the table, the variation ranges of the seven design variables dimensionless.

The optimized LHS design method is used to generate a total of 280 uniform and orthogonal sample points within the sample space formed by the seven design variables; the distribution of different design variables in the design space is shown in Fig. 9. Meanwhile, 280 new hull forms are achieved by means of the FFD method. Next, the wave-making resistance of each new hull form is evaluated. Finally, the Kriging model is employed to construct an approximate response function surface to represent the relationship between the objective function and the design variables.

3.2 Optimization results and analysis

With an initial population size of 200, a crossover rate of 0.8, a mutation rate of 0.2, and a maximum iteration number of 400, the multi-objective

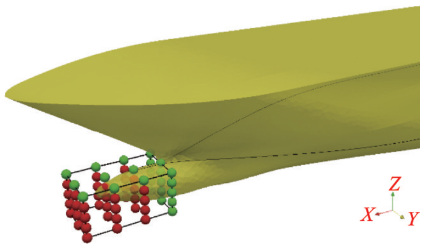

(a) Movement in the ship length direction at the bow (X_1)

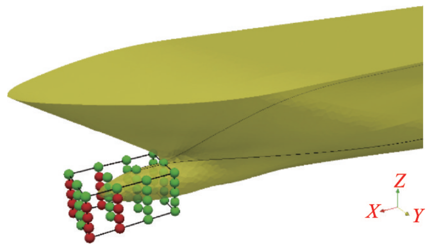

(b) Movement in the ship breadth direction at the bow (Y_1)

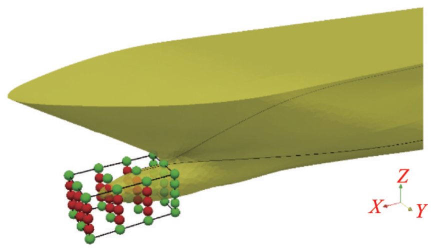

(c) Movement in the ship draft direction at the bow (Z_1)

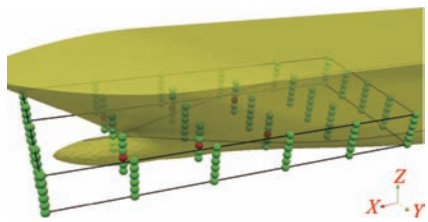

(d) Movement in the draft direction at the waterline (Y_2)

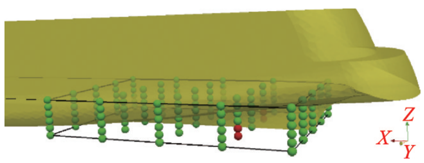

(e) Movement in the ship breadth direciton at the stern (Y_3)

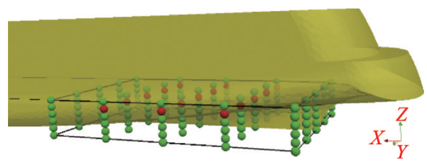

(f) Movement in the draft direction at the stern (Z_2)

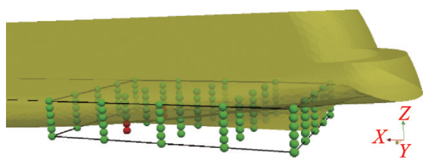

(e) Movement in the ship breath direciton at the stern (Y_4)

Fig. 8 Distribution of control points of FFD lattices

Table 2 Definition of optimization case

Item		Configuration information	Remarks
Objective function		$\min f_1 = C_w (Fr = 0.171\ 15)$	–
		$\min f_2 = C_w (Fr = 0.209\ 18)$	–
Design variable	X_1	[−0.015,0.015]	Movement in the ship length direction at the bow
	Y_1	[−0.01,0.01]	Movement in the ship breadth direction at the bow
	Z_1	[−0.005,0.005]	Movement in the draft direction at the bow
	Y_2	[−0.025,0.025]	Movement in the draft direction at the waterline
	Y_3	[−0.02,0.02]	Movement in the ship breadth direction at the stern
	Z_2	[−0.004,0.004]	Movement in the draft direction at the stern
	Y_4	[−0.02,0.02]	Movement in the ship breath direction at the stern
Wetted surface area and displacement constraint		Within ±1%	–
DoF method		Optimized LHS design	Sample quantity of 280
Optimization algorithm		NSGA-II	Population size of 200, number of generations of 400

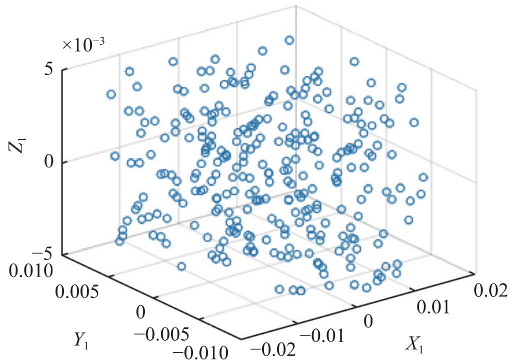

(a) The first three design variables

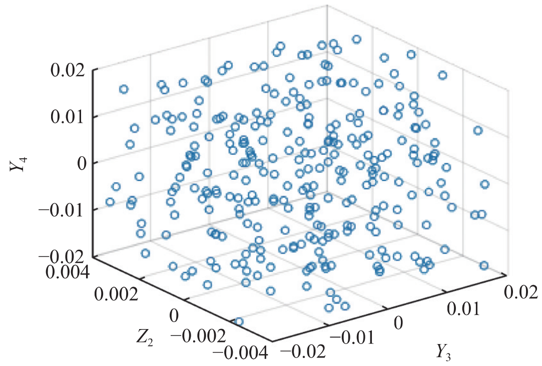

(b) The last three design variables

Fig. 9 Distribution of different design variables in the design space

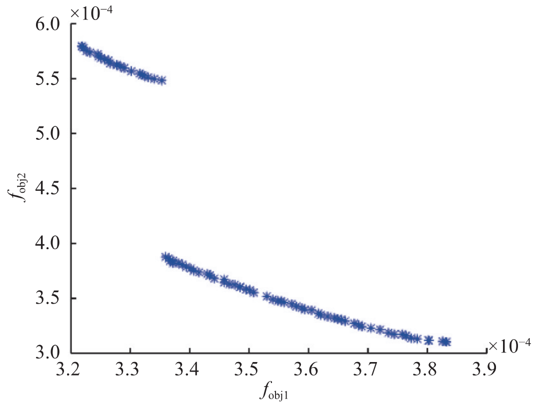

Fig. 10 Pareto front of wave-making resistance coefficient

genetic algorithm, NSGA-II, is used to search for the optimal solution. The eventually achieved Pareto front is shown in Fig. 10. In the figure, f_{obj1} and f_{obj2} stand for the wave-making resistance coefficients at lower and higher speeds, respectively, and the blue star points constitute the Pareto front achieved by the optimization algorithm. It can be seen that compared with a single-objective optimization problem, multi-objective optimization no longer seeks the only optimal solution, but a collection of a series of feasible solutions. The Pareto front forms a convex set, namely that compared with the Pareto solution, there are no other solutions that reduce the objective function f_1 while f_2 simultaneously decreases, or reduce f_2 while f_1 simultaneously decreases. Moreover, it can be seen that the wave-making resistance coefficients of the optimized hull forms of the Pareto front are negatively correlated at Fr= 0.171 15 and 0.209 18. In this work, two feasible solutions (OPT1 and OPT2) from the Pareto solution set, as shown in Table 3, are chosen to further analyze and verify the optimization results.

Fig. 11 compares the cross-section lines between the two optimized hull forms and the initial hull form. It can be seen that there is a big difference in the deformation between the bulbous blow and the stern, and the changes in the waterline of the inflow section are basically the same.

Based on the NM theory, the free-surface wave elevations of the two optimized hull forms (OPT1, OPT2) and the initial hull form are compared, and

Table 3 Design variable values of optimal hull forms

Design vriable values	OPT1(optimal at low *Fr*)	OPT2(optimal at high *Fr*)
X_1	0.005 5	0.000 8
Y_1	0.006 9	0.009 7
Z_1	−0.003 2	−0.003 2
Y_2	−0.024 0	−0.024 1
Y_3	−0.017 5	0.019 3
Z_2	−0.003 9	0.003 9
Y_4	0.019 8	−0.018 3

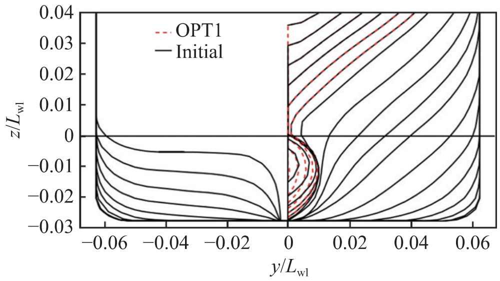

(a) Comparison of OPT1 and initial hull forms

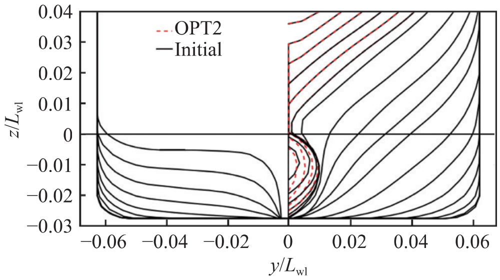

(b) Comparison of OPT2 and initial hull forms

Fig. 11 Comparison between optimal and initial hull forms

the results are shown in Fig. 12. It can be seen that due to the deformation of bulbous bow, the peaks and troughs of the bow waves of both the optimized hull forms are reduced at two cruise speeds, and the optimization effect of OPT1 is more noticeable.

In order to further verify the reliability of the optimization results, we evaluated the calm-water total resistances of the initial hull form and the two optimized hull forms at two speeds. The viscous flow solver, naoe-FOAM-SJTU [19−20], which has been independently developed based on the OpenFOAM

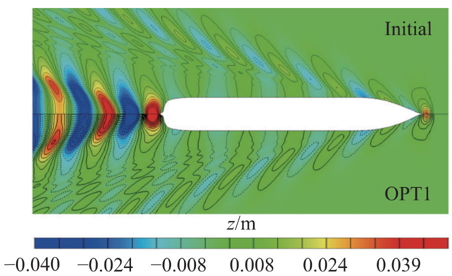

(a) Free-surface wave elevation of the OPT1 and initial hull forms (Fr=0.17115)

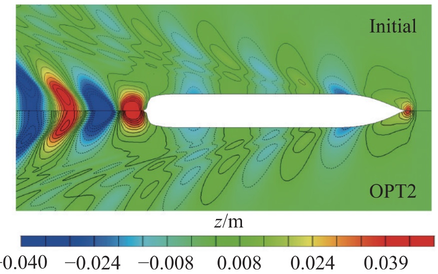

(b) Free-surface wave elevation of the OPT2 and initial hull forms (Fr=0.209 18)

Fig. 12 Comparison of wave elevation between optimal and initial hull forms by NMShip-SJTU

platform, is used as the evaluation tool. The solver includes a 6-DoF motion module and a numerical wave-making module, which can accurately forecast the ship's hydrodynamic performance such as rapidity, seakeeping ability, propulsion ability, and maneuverability, which can provide the fine characteristics of the flow field. Its reliability has been validated in many studies [19−20].

Based on the naoe-FOAM-SJTU solver, the distributions of the free-surface wave elevation z and the hull surface pressure p between the two optimized hull forms and the initial hull form are obtained and shown in Fig. 13. It can be seen that for OPT1, wave elevation at the bow is somewhat reduced, and the high-pressure zone of the bow is slightly decreased; for OPT2, the wave elevation at the parallel midbody is somewhat decreased, and the high-pressure zone of the bow is significantly

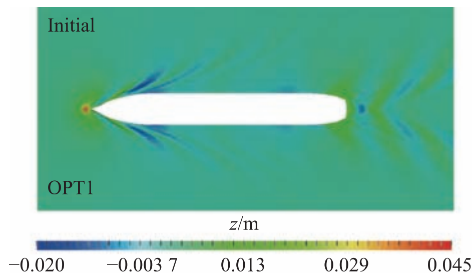

(a) Surface pressure distribution of the OPT1 and initial hull forms (Fr=0.171 15)

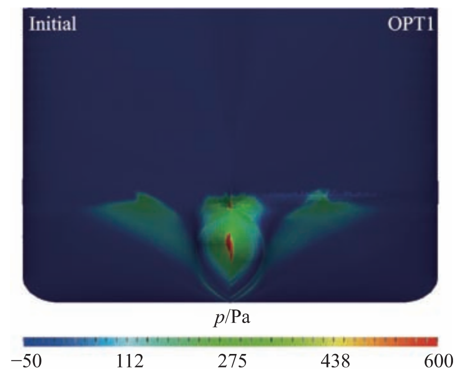

(b) Free-surface wave elevation ot the OPT1 and initial hull forms (Fr=0.171 15)

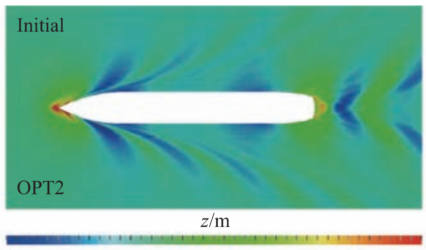

(c) Surface pressure distribution of the OPT2 and initial hull forms (Fr=0.209 18)

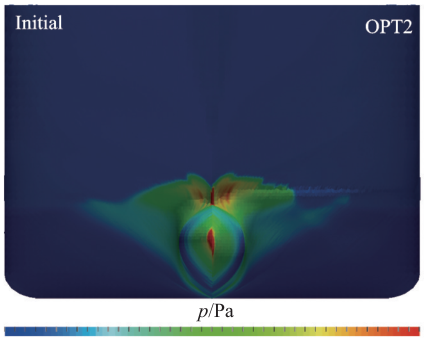

(d) Free-surface wave elevation ot the OPT2 and initial hull forms (Fr=0.209 18)

Fig. 13 Comparison of wave elevation and hull surface pressure distribution between optimal and initial hull forms by naoeFOAM-SJTU

reduced.

Table 4 and Table 5 compare the evaluation results of the total resistance of the two optimized hull forms and the initial hull form, respectively. It can be seen from the tables that for the optimized hull forms obtained on the basis of potential flow evaluation, their pressure resistance in the total resistance is significantly reduced, indicating that the optimized hull forms obtained from the NM theory-based evaluation are reliable, and their total resistance is lower than that of the initial hull form when the frictional resistance is almost constant. In fact, the effect of viscosity has not been considered in this paper when the potential flow theory based solver is used; therefore, the optimization target is the wave-making resistance at different speeds, and the optimization range is relatively large from the perspective of the optimization effect on wave-making resistance. What corresponds to the wave-making resistance is the component of pressure resistance in the total resistance achieved by the viscous flow solver, and it can also be seen from the result of pressure resistance that it reflects the potential flow-based optimization effect from the side. In the subsequent verification, validations by model testing or other commercial software can be supplemented to further illustrate the reliability of the method in this work. The aforementioned results show that the wave-making resistance optimization based on NM theory can obtain hull forms with better overall resistance performance; the optimization is more efficient and exhibits higher application value compared with viscous flow-based CFD evaluation.

Table 4 Comparison of total resistance between initial and OPT1 hull forms at Fr = 0.171 15

Resistance component	Initial huu form	OPT1	Degree of reduction/%
Pressure resistance/N	2.76	2.48	9.99
Frictional resistance/N	24.98	25.07	−0.38
Total resistance/N	27.69	27.30	0.65

Table 5 Comparison of total resistance between initial and OPT2 hull forms at Fr = 0.209 18

Resistance component	Initial huu form	OPT2	Degree of reduction/%
Pressure resistance/N	4.54	4.16	8.27
Frictional resistance/N	35.47	35.46	0.04
Total resistance/N	40.01	39.62	0.98

4 Conclusions

In this work, the hull form optimization software, OPTShip-SJTU, is used to optimize the resistance performance of a luxury cruise ship. First of all, the method to obtain a new hull form by rationally deforming the hull is analyzed in accordance with the characteristics and design requirements of the luxury cruise ship; then, the NMShip-SJTU solver is employed to calculate the wave-making resistance coefficient of each new hull form by using the results of optimized LHS design; finally, the multi-objective wave-making resistance coefficient of the luxury cruise ship at two speeds optimization is implemented and further verified by establishing an approximation response function model and using the NSGA-II optimization algorithm. The results show that the method to optimize the calm-water wave-making resistance performance of the ship, which is based on the evaluation of the potential flow theory, is highly efficient, and the results can be verified by the results of viscous flow evaluation. The OPTShip-SJTU solver can be widely used in the optimization of the resistance performance of the practical hull forms of luxury cruise ships, and the reduction effect on the total resistance at two calculated speeds reaches 0.65% and 0.98%, respectively.

Based on the real demands and the characteristics of a luxury cruise ship, the stability optimization for its high superstructure and poor stability, the principal dimension optimization for the aesthetic needs of its appearance, as well as the sea-keeping optimization for the comfort of tourists, the convenience of sightseeing, and the prevention of seasickness can also be taken into account in the future.

References

[1] ZHANG X Z, WANG C M, GUO A. New design of bulbous for luxury cruise ship [J]. Ship Engineering, 2014, 36 (Supp 1): 12−15 (in Chinese).

[2] WANG S, WANG Y X, ZHAO Q, et al. Bulbous bow optimization for a medium-sized luxury cruise based on parametric design method [J]. Journal of Jiangsu University of Science and Technology (Natural Science Edition), 2017, 31 (5): 646−649 (in Chinese).

[3] WANG Y X, PENG B Y, ZHAO Q. Experimental study on the influence of trim flap on the resistance of a medium-sized luxury cruise [J]. Chinese Journal of Hydrodynamics (Ser. A), 2017, 32 (6): 725−731 (in Chinese).

[4] YANG Z Z, ZHU X C. Optimization of costal cruise line oriented to requirements of middle class [J]. Navigation of China, 2014, 37 (4): 105−109, 119 (in Chinese).

[5] XU Z L. The research on the route optimization of Shanghai cruise homeport [D]. Shanghai: Shanghai University of Engineering Science, 2015 (in Chinese).

[6] SUN L, JIN Q. On the key issues in general design of cruise ship [J]. Ship & Ocean Engineering, 2019, 48 (3): 10−14 (in Chinese).

[7] TONG C, CHEN D W. Layout study of elevator/elevator hall of luxury cruise ships [J]. Journal of Ship Design, 2018 (2): 26−32 (in Chinese).

[8] IMO. International convention for the safety of life at sea [S]. London, UK: IMO, 2009.

[9] LR. Safe return to port requirements and compliance [S]. UK: LR, 2012.

[10] HARRIES S. Parametric design and hydrodynamic optimization of ship hull forms [D]. Berlin, Germany: Technische Universität Berlin, 1998.

[11] PERI D, PINTO A, CAMPANA E F. Multi-objective optimization of expensive objective functions with variable fidelity models [M]//DI PILLO G, ROMA M. Large-Scale Nonlinear Optimization. Boston, MA: Springer, 2006: 223−241.

[12] CAMPANA E F, DIEZ M, IEMMA U, et al. Derivative-free global ship design optimization using global/local hybridization of the DIRECT algorithm [J]. Optimization and Engineering, 2016, 17 (1): 127−156.

[13] HUANG F X, YANG C. Hull form optimization of a cargo ship for reduced drag [J]. Journal of Hydrodynamics, 2016, 28 (2): 173−183.

[14] LIU X W, WANG J K, WAN D C. Hull form optimization design of KCS at full speed range based on resistance performance in calm water [C]//Proceedings of the 28th International Ocean and Polar Engineering Conference. Sapporo, Japan: ISOPE, 2018: 626−632.

[15] LIU X W, WAN D C, CHEN G, et al. Wigley hull form optimization with or without bulbous bow [C]//Proceedings of the 29th International Ocean and Polar Engineering Conference. Honolulu, HI, USA: ISOPE, 2019: 4486−4493.

[16] SEDERBERG T W, PARRY S R. Free-form deformation of solid geometric models [J]. ACM SIGGRAPH Computer Graphics, 1986, 20 (4): 151−160.

[17] NOBLESSE F, HUANG F X, YANG C. The Neumann - Michell theory of ship waves [J]. Journal of Engineering Mathematics, 2013, 79 (1): 51−71.

[18] DEB K, PRATAP A, AGARWAL S, et al. A fast and elitist multiobjective genetic algorithm: NSGA-II [J]. IEEE Transactions on Evolutionary Computation, 2002, 6 (2): 182−197.

[19] YE H X, SHEN Z R, WAN D C. Numerical prediction of added resistance and vertical ship motions in regular head waves [J]. Journal of Marine Science and Application, 2012, 11 (4): 410−416.

[20] SHEN Z R, WAN D C, CARRICA P M. Dynamic overset grids in OpenFOAM with application to KCS self-propulsion and maneuvering [J]. Ocean Engineering, 2015, 108: 287−306.

[*Continued on page* 30]

基于SOLAS 2020概率破舱稳性要求的中型邮轮优化措施研究

王晓强[1], 李鹏[*2]
1 海军装备部驻武汉地区第二军事代表室, 湖北 武汉 430064
2 中国舰船研究设计中心, 湖北 武汉 430064

摘　要: [目的] 破舱稳性是保障船舶稳性的重要性能之一, SOLAS 2020 对客船分舱指数 R 的要求大幅提升, 因此需要关注邮轮的概率破舱稳性。[方法] 以某中型邮轮为对象, 对比分析 SOLAS 2020 和 SOLAS 2009 中所要求的分舱指数 *R*; 采用 Maxsurf 软件对初始方案进行概率破舱计算; 通过对达到的分舱指数 A 的影响因素分析, 提出沿纵向加密分舱、设置横贯进水装置、降低重心高这 3 种改进措施, 并对改进方案进行分析。[结果] 结果表明, 所达到的分舱指数 *A* 与 SOLAS 2020 中要求的 *R* 差距较大。与 SOLAS 2009 相比, SOLAS 2020 对载客量约 1 250 人的某中型邮轮的 *R* 提升了约 13.6%。设置横贯进水装置对 A 的改善效果达到 10% 以上, 采用沿纵向加密分舱对 *A* 的的改善效果达到 8.7%; 由于初始 *GM* 值较大, 采用降低重心高对 *A* 的改善效果较弱。而采用改进措施的组合方案, 可使中型邮轮满足 SOLAS 2020 的分舱指数 *R* 的要求。[结论] 对于初始 *GM* 较大的中型邮轮, 设置横贯进水装置的改善效果最佳, 沿纵向加密分舱次之, 降低重心高效果较弱。
关键词: 邮轮; SOLAS 2020; 概率破舱稳性

[*Continued from page* 13]

豪华邮轮多航速兴波阻力的船型优化

刘鑫旺[1,2,3], 万德成[*1,2,3]
1 上海交通大学 船舶海洋与建筑工程学院, 上海 200240
2 上海交通大学 海洋工程国家重点实验室, 上海 200240
3 上海交通大学 船海计算水动力学研究中心, 上海 200240

摘　要: [目的] 豪华邮轮的型线优化设计, 除了要考虑美学视角因素, 更重要的是还要考虑在整个航行阶段都能满足绿色节能、安全舒适等方面的要求, 其中针对多航速船舶阻力性能优化进行豪华邮轮的船型设计尤为重要。[方法] 首先, 基于自主开发的船型优化设计软件 OPTShip-SJTU, 以某豪华邮轮为原始船型, 通过自由变形方法, 对船艏、水线、船艉等位置进行局部变形; 然后, 通过基于 Neumann-Michell (NM) 势流理论的兴波阻力求解器 NMShip-SJTU 进行阻力评估, 并结合优化算法得到不同航速下兴波阻力系数最优的船型; 最后, 采用经过广泛验证的高精度黏流求解器 naoe-FOAM-SJTU 对优化船型做进一步验证。[结果] 结果显示, 基于 NM 势流理论的兴波阻力优化可以得到多航速下总阻力性能更优的船型, 相比基于黏流 CFD 评估进行优化, 更高效, 且得到的优化船型在 2 个航速下总阻力分别降低了 0.65% 和 0.98%。[结论] 研究表明, 基于数值模拟的船型优化设计流程可以应用于豪华邮轮的阻力性能优化。
关键词: 豪华邮轮; 多航速船型优化; 兴波阻力; OPTShip-SJTU; NM 势流理论; naoe-FOAM-SJTU